Modeling of pulsed finite-amplitude focused sound beams in time domain

Jahangir Tavakkoli,[a] Dominique Cathignol, and Rémi Souchon
INSERM—Unité 281, 151 Cours Albert Thomas, 69424 Lyon Cedex 03, France

Oleg A. Sapozhnikov
Department of Acoustics, Physics Faculty, Moscow State University, Moscow 119899, Russia

(Received 10 June 1997; revised 11 June 1998; accepted 23 June 1998)

A time-domain numerical model is presented for simulating the finite-amplitude focused acoustic pulse propagation in a dissipative and nonlinear medium with a symmetrical source geometry. In this method, the main effects responsible in finite-amplitude wave propagation, i.e., diffraction, nonlinearity, and absorption, are taken into account. These effects are treated independently using the method of fractional steps with a second-order operator-splitting algorithm. In this method, the acoustic beam propagates, plane-by-plane, from the surface of a highly focused radiator up to its focus. The results of calculations in an ideal (linear and nondissipative) medium show the validity of the model for simulating the effect of diffraction in highly focused pulse propagation. For real media, very good agreement was obtained in the shape of the theoretical and experimental pressure-time waveforms. A discrepancy in the amplitudes was observed with a maximum of around 20%, which can be explained by existing sources of error in our measurements and on the assumptions inherent in our theoretical model. The model has certain advantages over other time-domain methods previously reported in that it: (1) allows for arbitrary absorption and dispersion, and (2) makes use of full diffraction formulation. The latter point is particularly important for studying intense sources with high focusing gains. © *1998 Acoustical Society of America.* [S0001-4966(98)02810-0]

PACS numbers: 43.25.Jh [MAB]

INTRODUCTION

Advances in the development of acoustic microscopes,[1] high intensity focused ultrasound surgery,[2] lithotripsy, and cavitation-induced tissue destruction[3] have generated renewed concern about finite-amplitude effects in focused sound beams. Each system is capable of transmitting focused sound that is strongly affected by the combined influence of nonlinearity, absorption, and diffraction. Existing analytical solutions fail to adequately describe these sound fields, and only recently have numerical solutions been developed that model the radiation of focused finite-amplitude sound from practical sources.

A series of theoretical models for studying the focusing of intensive acoustic waves has been developed during the last two decades. A model which seems to be best suited to the study of moderately focused acoustic beams and which accounts for diffraction, nonlinearity, and absorption is based on the Khokhlov–Zabolotskaya–Kuznetsov (KZK) parabolic equation.[4,5] In the original KZK equation, the effect of absorption is modeled by incorporating viscous and thermal conductivity losses, in which the absorption coefficient is assumed to be proportional to the square of frequency. However, such an assumption is not appropriate to most biological tissues which exhibit a nearly linear frequency dependence. Concerning the diffraction effect, the KZK model uses a so-called parabolic or quasi-optical approximation, which means that the angular spectrum is supposed to be narrow or, in other words, the wave is very close to a plane wave. This is not the case for strongly focused beams or for beams with strong irregularities in the transverse structure, e.g., near the edges or at the focal point of a focused source. This limits the validity of the model to the cases in which diffraction effects are relatively weak and focusing gains are relatively low. In general, the KZK equation is an accurate model of the sound field produced by directional sound sources ($ka \gg 1$, where k is the wave number and a the radius of the source) at distances beyond a few source radii and in the paraxial region. A complete discussion of the domain of validity of the KZK equation for plane and focused sources is provided in Refs. 6 and 7.

A number of computer algorithms has been proposed to solve the KZK equation numerically. One of the most popular algorithms for solving the KZK equation is a frequency-domain technique, called the spectral method, introduced by Aanonsen[8] and co-workers.[9] Most studies, based on the spectral method, focused initially on monochromatic waves or on tone bursts. However, in many biomedical applications the acoustic wave consists of a small number of cycles or even has the form of a single cycle. If, additionally, shock fronts are developed because of nonlinearity, the numerical analysis requires large amounts of computer time. The situation becomes even more complex if the absorption is frequency dependent and the beam is strongly focused.

To partially overcome these problems, Lee and Hamilton[10] developed a time-domain algorithm for solving the KZK equation. A marching scheme, based on the

[a]Current address: Institute of Biomedical Eng., University of Toronto, 4 Taddle Creek Road, Toronto, Ontario M5S 3G9, Canada.

operator-splitting method,[11,12] was used as the basis for the algorithm. In this technique, as the code marches along, at each step it takes separate account of nonlinear distortion, absorption, dispersion, diffraction, and any other effects. Cleveland *et al.*[13] used this algorithm to solve an augmented KZK equation that accounts for nonlinearity, thermoviscous absorption, relaxation, and diffraction in directive sound beams. Moreover, Averkiou and Hamilton[14] have recently presented new results of this time-domain model for the case of short pulses radiated by plane and focused circular pistons. Within the limits of the KZK model, they obtained very good agreement between their simulations and experiments.

In a related work, again based on the operator-splitting method, Cleveland *et al.*[15] presented a comparison of several time and frequency-domain codes for the propagation of sonic booms through idealized atmosphere. The main effects considered in these codes were nonlinearity, absorption, and dispersion.

A model of nonlinear diffractive field propagation, not based on the KZK equation, was developed by Christopher and Parker.[16] In this model, using an operator-splitting method, they solved the equations of diffraction and absorption in the frequency domain and the equation of nonlinearity in the time domain. This model has advantages over the KZK model in that it accounts for full diffraction and arbitrary absorption effects. Using a modified version of this model, Christopher[17] presented the modeling of an electrohydraulic, extracorporeal shock wave lithotripter as an example of an intense highly focused sound source.

On the other hand, the effect of acoustic nonlinearity on the focused beam can be predicted on the basis of simpler theoretical approaches. We have already proposed a simple model that makes it possible to study the focusing of an intense pulse on the basis of the spherical wave theory.[18] In this model, the focusing is associated with wave propagation along a rigid-wall tube. The dependence of the tube cross section on distance is chosen in such a way that the peak pulse pressure in the tube coincides with the peak pressure calculated by the Rayleigh diffraction integral in the linear regime. The nonlinear wave propagation along the tube is then described on the basis of a Burgers-type equation. Of course, such a simple model suffers from the same limitations as nonlinear spherical wave theory and is not accurate enough, especially in the focal region of a high-amplitude focused source. For this reason, we present another, more complete, model. As with the approach used by Christopher, our model accounts for full diffraction and arbitrary absorption effects. A second-order operator-splitting algorithm is used to solve a set of equations that account for the effects of diffraction, absorption, and nonlinearity. To avoid numerical errors associated with the transformations between the time and frequency domains, a pure time-domain approach has been adopted.[15] The basic theoretical approach and the results obtained are presented below. The model was used for simulating the pressure field of a highly focused source developed for tissue destruction studies.[19]

I. BASIC EQUATIONS

In general wave theory, differential equations of the evolution type are widely used to describe the propagation process:

$$\frac{\partial v(\tau,z)}{\partial z} \equiv \hat{L}\cdot v, \tag{1}$$

where v is the particle velocity, z is the coordinate in the direction of wave propagation, $\tau = t - z/c_0$ is retarded time, c_0 is the wave speed, and the operator $\hat{L}$ accounts for the effects changing the waveform. If $\hat{L}\cdot v = 0$, we have $v = F(\tau)$, i.e., the waveform does not change during propagation, which is the case of a plane wave traveling in an ideal linear medium. In reality, the waveform is distorted due to different effects. Consider, for instance, the equation for a linear plane acoustic wave propagating in a thermoviscous medium:[20]

$$\frac{\partial v}{\partial z} = \frac{b}{2\rho_0 c_0^3}\frac{\partial^2 v}{\partial \tau^2}, \tag{2}$$

where b is the dissipative coefficient of the medium and ρ_0 is the ambient density. In many practical situations, e.g., in biological tissues, the attenuation operator differs from that of Eq. (2). It can be written in the general form:[21]

$$\frac{\partial v}{\partial z} = \int_{-\infty}^{\tau} K(z,\tau-\tau')\cdot v(z,\tau')\,d\tau' \equiv \hat{L}_A\cdot v, \tag{3}$$

where the kernel K can be evaluated from the frequency dependence of the attenuation. The upper limit of the integral accounts for causality.

Another example is the evolution equation for a plane wave propagating in a lossless quadratically nonlinear medium:

$$\frac{\partial v}{\partial z} = \frac{\beta}{c_0^2}\, v\, \frac{\partial v}{\partial \tau} \equiv \hat{L}_N\cdot v, \tag{4}$$

where β is the coefficient of nonlinearity of the medium.

The third example is the so-called parabolic equation, describing diffraction of acoustical beams in linear lossless medium:

$$\frac{\partial v}{\partial z} = \frac{c_0}{2}\nabla_\perp^2 \int_{-\infty}^{\tau} v\; d\tau', \tag{5}$$

where z is the distance along the beam axis, $\nabla_\perp^2$ is a two-dimensional transverse Laplacian, and v is the axial component of particle velocity. Equation (5) describes the effect of diffraction properly only if the wave angular spectrum is narrow (quasi-plane wave). A more exact, wider-angle parabolic evolution equation was proposed by Hill.[22] On the other hand, the diffraction effect can be described by the Rayleigh integral over the initial source surface.[23] It is known that the Rayleigh integral presents an exact solution of the diffraction problem for the case of a plane surface. When the surface is curved, the integral gives an approximate, but fairly accurate solution.[24,25] Let us denote the corresponding diffraction operator as $\hat{L}_D$ and write a general form of the evolution equation for diffraction:

$$\frac{\partial v}{\partial z}=\hat{L}_D\cdot v. \tag{6}$$

In all of the above examples, each evolution equation is associated with only one effect. In the presence of multiple effects, if each is fairly weak, the evolution equation can be derived simply by summing the corresponding operators from the ''one-effect equations'':

$$\frac{\partial v}{\partial z}=\sum_{i=1}^{N}\hat{L}_i\cdot v. \tag{7}$$

For example, the combination of Eqs. (2) and (4) gives the Burgers equation and the combination of Eqs. (2), (4), and (5) results in the KZK equation. A more exact result than the KZK equation, accounting for the absorption and diffraction effects, is possible on the basis of combining Eqs. (3), (4), and (6). We write this combined equation in a general form:

$$\frac{\partial v}{\partial z}=\hat{L}\cdot v\equiv\hat{L}_A\cdot v+\hat{L}_N\cdot v+\hat{L}_D\cdot v, \tag{8}$$

which will be used for the development of our model for finite-amplitude acoustic pulse focusing. Note that $\hat{L}$ is a fairly complex integro-differential operator. One of the possible ways of solving it numerically is the use of the method of fractional steps with an operator-splitting procedure.[11,12] According to this method, the solution of the Eq. (8) at each step Δz is obtained on the basis of separate solutions of Eqs. (3), (4), and (6). This is why we will first consider each of these equations separately.

II. SOLVING THE ABSORPTION EQUATION

A. Minimum-phase digital filter model for absorption and dispersion

Here, a causal FIR (finite impulse response) digital filter for simulating the effects of frequency-dependent absorption and dispersion is presented. Let us consider Eq. (3) as accounting for dispersion and frequency-dependent absorption. After passing through the layer Δz, each spectral component $e^{i\omega\tau}$ changes its amplitude by a factor:

$$G_a(\Delta z,\omega)=\exp\{-\alpha(\omega)\cdot\Delta z+i\omega[c^{-1}(\omega)-c_0^{-1}]\cdot\Delta z\}, \tag{9}$$

where i is the imaginary unit, $c(\omega)$ is sound speed, $\alpha(\omega)$ is the absorption coefficient of the medium, and $\omega=2\pi f$ is angular frequency. The waveform v at distance $z+\Delta z$ can be evaluated from the waveform at distance z by a convolution integral:

$$v(z+\Delta z,\tau)=\int_{-\infty}^{+\infty}v(z,\tau')\cdot g(\Delta z,\tau-\tau')d\tau', \tag{10}$$

where the impulse response g is an inverse Fourier transform of the factor G_a:

$$g(\Delta z,\tau)=\frac{1}{2\pi}\int_{-\infty}^{+\infty}G_a(\Delta z,\omega)e^{i\omega\tau}\,d\omega. \tag{11}$$

The discrete analogy of the convolution integral (10) has the form of a convolution sum:

$$v_n(z+\Delta z)=\sum_{k=-\infty}^{+\infty}v_k(z)\cdot g_{n-k}(\Delta z), \tag{12}$$

where $v_n(z)=v(z,nT)$, $g_n(\Delta z)=T\cdot g(\Delta z,nT)$, and T is a uniform time-sampling period. In discrete regime, the Fourier integral (11) transforms to:

$$g_n(\Delta z)=\frac{1}{2\pi}\int_{-\pi}^{\pi}G(e^{i\Omega})e^{i\Omega n}\,d\Omega, \tag{13}$$

where

$$G(e^{i\Omega})=\frac{1}{T}\sum_{k=-\infty}^{+\infty}G_a\left(\Delta z,\frac{\Omega+2\pi k}{T}\right)$$

is a periodic function with a period of 2π, associated with the frequency response.[26] Supposing that $G_a=0$ for $\omega>2\pi/T$, we can therefore use within the interval $-\pi\leqslant\Omega\leqslant\pi$:

$$G(e^{i\Omega})=\frac{1}{T}G_a\left(\Delta z,\omega=\frac{\Omega}{T}\right). \tag{14}$$

The complex function $G(e^{i\Omega})$ can be considered to be a transfer function of a digital attenuater filter. Taking causality into account, the argument of $G(e^{i\Omega})$ is related to its magnitude by the minimum-phase condition. It is well known that for a minimum-phase filter, the log-magnitude and phase characteristics form a Hilbert transform pair.[26] Using the discrete-time Hilbert transform, the phase of the filter is equal to:

$$\arg[G(e^{i\Omega})]=\frac{1}{2\pi}P\int_{-\pi}^{\pi}\ln|G(e^{i\theta})|\cdot\cot\left(\frac{\theta-\Omega}{2}\right)d\theta, \tag{15}$$

where the symbol P denotes the Cauchy principal value of the integral. It is to be noted that as $T\to 0$, Eq. (15) transforms into the Kramers–Kronig relation between the attenuation coefficient and phase velocity.[27] Integral (15) can be rewritten in the following form:

$$\arg[G(e^{i\Omega})]=-\frac{1}{\pi}\int_0^{\pi}\frac{d[\ln|G(e^{i\theta})|]}{d\theta}\cdot\ln\left|\frac{\sin[(\theta+\Omega)/2]}{\sin[(\theta-\Omega)/2]}\right|d\theta. \tag{16}$$

The logarithmic singularity here does not need the Cauchy principal value integration. Using Eq. (16), it is possible to obtain the unit-sample response of the attenuater filter based only on the frequency dependence of the absorption coefficient $\alpha(\omega)$. Indeed, according to Eq. (14):

$$|G(e^{i\Omega})|=\frac{1}{T}\exp[-\alpha(\Omega/T)\cdot\Delta z]. \tag{17}$$

According to Eq. (16), the argument of G is also related to the function $\alpha(\omega)$:

$$\arg[G(e^{i\Omega})]=\frac{\Delta z}{\pi T}\int_0^{\pi}\dot{\alpha}(\theta/T)\cdot\ln\left|\frac{\sin[(\theta+\Omega)/2]}{\sin[(\theta-\Omega)/2]}\right|d\theta, \tag{18}$$

where $\dot{\alpha}(\omega)=d\alpha/d\omega$. Equations (17) and (18) give the complex function $G(e^{i\Omega})$. Based on this, the unit-sample response can be calculated from Eq. (13). The waveform after passing the layer Δz can be calculated from the convolution sum of Eq. (12). As the unit-sample response is a causal sequence, this sum is started from $k=0$.

To minimize the numerical errors induced by the FFT operations,[15] we chose to apply absorption by means of a convolution with an FIR filter in the time domain. For a waveform with M samples, the computation time for a convolution operation is proportional to M^2, whereas the time for an FFT operation is proportional to $M\cdot\log M$ (if M is not an integer power of 2, the computation time for an FFT operation is slightly higher). However, the absorption calculation takes up only a small portion of the total computation time in our algorithm (more than 80% of the total computation time is for the diffraction calculation). Using convolution for the absorption calculation does not, therefore, have a major influence on the total computation time.

B. Acoustic absorption in biological tissue

The acoustic absorption coefficient of soft tissue, when expressed in logarithmic units such as dB/cm, has been observed to increase approximately linearly with frequency. In order to simulate this absorption characteristic on a digital computer, a minimum-phase digital filter model was developed in Sec. II A. It has been argued that this filter model is appropriate for describing a physical medium exhibiting a linear-with-frequency absorption such as soft tissues.[28,29] Let the absorption coefficient of the medium, denoted by $\alpha(f)$, be a linear function of frequency (in MHz) with slope α_0:

$$\alpha(f)=\alpha_0\cdot f \quad \text{dB/cm}. \tag{19}$$

The log-magnitude transfer function of the attenuater filter for a Δz cm thick section of the medium, denoted by $L(f)$, is equal to

$$L(f)=-\alpha(f)\cdot\Delta z=-\alpha_0\cdot f\cdot\Delta z \quad \text{dB}. \tag{20}$$

The resulting magnitude function, denoted by $|G(f)|$, is then equal to

$$|G(f)|=10^{L(f)/20}=10^{-\alpha_0 f\Delta z/20}. \tag{21}$$

Now, using this magnitude function in Eq. (16) results in the phase function, and consequently, the complex transfer function of the minimum-phase filter:

$$G(f)=|G(f)|\cdot\exp\{i\cdot\arg[G(f)]\}. \tag{22}$$

The unit-sample response of the filter which is used for the convolution sum is equal to the real component of the inverse Fourier transform obtained from Eq. (13). Note that the imaginary component should be zero for a physical filter.

An example of implementation of this filter for simulating the absorption of acoustic pulses in liver tissue is shown in Fig. 1. In this example, the coefficient of absorption in the liver, α_0, was set equal to 0.5 dB $\text{cm}^{-1}\,\text{MHz}^{-1}$, and the distance Δz to 5 cm. Figure 1(a) and (b) shows the magnitude of the filter transfer function in linear and in logarithmic units respectively, and Fig. 1(c) shows its phase obtained from the Hilbert transform. The unit-sample response of the filter is shown in Fig. 1(d). Verification of the results obtained by applying this filter to a monochromatic sinusoidal wave demonstrated that it is possible to simulate exactly the frequency-dependent absorption of biological tissues.[28,30]

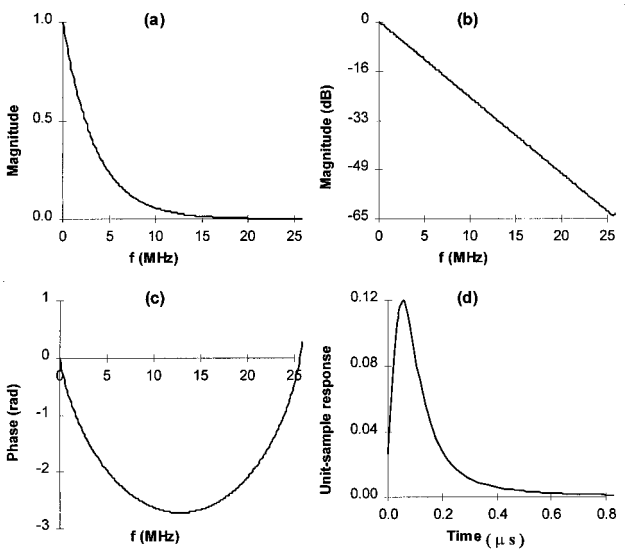

FIG. 1. Characteristics of the minimum-phase digital filter with $\alpha_0=0.5$ dB $\text{cm}^{-1}\,\text{MHz}^{-1}$ and $\Delta z=5$ cm. (a) Magnitude of the filter transfer function; (b) log magnitude of the filter; (c) phase of the filter obtained from Hilbert transform; (d) unit-sample response of the filter.

III. SOLVING THE NONLINEARITY EQUATION

The Eq. (4) for a nonlinear medium has an analytical solution, called the Poisson or the Earnshaw solution. This solution, with a second-order approximation, can be written as (see, e.g., Ref. 31, Chap. 4):

$$v(z,\tau)=\Psi(\tau+\beta v z/c_0^2), \tag{23}$$

where $\Psi(t)$ is the waveform at $z=0$. To describe the nonlinearly induced wave distortion during its propagation from z to $z+\Delta z$, this solution may be rewritten as:

$$v(z+\Delta z,\tau)=v\left\{z,\tau+\frac{\beta\Delta z}{c_0^2}\,v(z,\tau)\right\}. \tag{24}$$

Multivalued solutions are avoided if

$$\Delta z<\frac{c_0^2/\beta}{\max(\partial v/\partial\tau)}. \tag{25}$$

Solution (24) can also be easily obtained using the nonlinear theory of acoustic waves.[32] The nonlinearity equation (4) can be solved in discrete regime via a time-base transformation on the basis of Eq. (24):

$$\tau_m^{n+1}=\tau_m^n-\frac{\beta\Delta z_n}{c_0^2}\cdot v_m^n, \tag{26}$$

where m marks the mth sample of the temporal waveform and n denotes the nth step Δz_n in z. The discrete analogy of the inequality (25) has a form of:

$$\Delta z_n<T\cdot\frac{c_0^2/\beta}{\max(v_m^n-v_{m-1}^n)}, \tag{27}$$

where $T=\tau_m^n-\tau_{m-1}^n$. After calculating of τ_m^{n+1}, linear interpolation is used to resample the waveform and thus reestablish a uniform time sample spacing T.[33]

The necessary condition for avoiding multivalued solutions requires a trade-off between the maximum of particle velocity variation and the propagation length Δz. It means that as the degree of wave distortion increases during its propagation in the medium, smaller distances are needed. To fulfill this requirement a nonuniform plane spacing was adopted in our model. Detailed description of the grid generation is presented in Sec. V.

IV. SOLVING THE DIFFRACTION EQUATION

From the classical theory of sound for a linear and nondissipative medium, the instantaneous pressure $p(\mathbf{r},t)$ and particle velocity $v(\mathbf{r},t)$ at a point $P(\mathbf{r})$ and time t in the field of an ultrasound source can be expressed as:[23]

$$p(\mathbf{r},t)=\rho\,\frac{\partial\phi}{\partial t}\,(\mathbf{r},t), \tag{28}$$

$$v(\mathbf{r},t)=-\nabla\phi(\mathbf{r},t), \tag{29}$$

where ρ is the equilibrium density of the surrounding medium,

$$\nabla=\frac{\partial}{\partial x}\,\mathbf{i}+\frac{\partial}{\partial y}\,\mathbf{j}+\frac{\partial}{\partial z}\,\mathbf{k}$$

is the gradient operator, and $\phi(\mathbf{r},t)$ denotes the velocity potential.

For the case of a uniformly excited planar radiator of area S in an infinite rigid baffle, $\phi(\mathbf{r},t)$ is given by the Rayleigh integral:

$$\phi(\mathbf{r},t)=\frac{1}{2\pi}\int\int_S\frac{v_0(t-r'/c_0)}{r'}\,ds, \tag{30}$$

where $v_0(t)$ is the instantaneous normal particle velocity at the source and r' is the distance between the observation point P and the surface element ds at the source.

When the shape of the source is not plane, but convex or concave, the wave radiated by the source is diffracted by its own surface. This secondary radiation contributes theoretically to the pressure field but is not taken into account by Eq. (30). However, this equation can be used as an excellent approximation for most practical applications, where the diameter of the source is large compared to the ultrasound wavelength, and the source is only slightly curved.[24,25] Under these conditions, for a spherical focused source, the Rayleigh integral has to be evaluated over the spherical concave surface of the source. The geometry used for applying the Rayleigh integral is shown in Fig. 2 with the origin of coordinates at the focal point of the source. Let point P belongs to a planar intermediate surface that is normal to the z axis. Based on Eq. (30) for the Rayleigh integral, we can calculate the velocity potential at each point on this plane. Then, using Eqs. (28) and (29), the values of pressure and particle velocity can be calculated for each point.

Further, for implementing our fractional-step method, we need the value of normal particle velocity at each point of the intermediate plane. Based on Eqs. (29) and (30) we can derive the Rayleigh integral for normal particle velocity v_n at point P of the observing plane as follows:

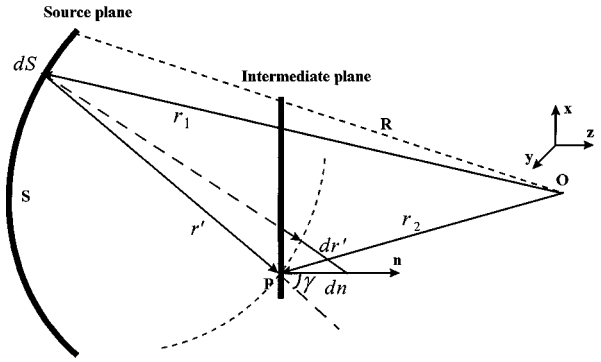

FIG. 2. Focused sound geometry used for calculation of the Rayleigh diffraction integral.

$$\begin{aligned}
v_n(\mathbf{r}_2,t)&=-\frac{\partial\phi}{\partial n}\\
&=-\frac{1}{2\pi}\int\int_S\frac{\partial}{\partial n}\left[\frac{1}{r'}\cdot v_n\left(\mathbf{r}_1,t-\frac{r'}{c_0}\right)\right]ds\\
&=-\frac{1}{2\pi}\int\int_S\left[\left(\frac{1}{r'}\right)\cdot\frac{\partial}{\partial t}\,v_n\left(\mathbf{r}_1,t-\frac{r'}{c_0}\right)\right.\\
&\quad\left.\cdot\frac{\partial}{\partial n}\left(-\frac{r'}{c_0}\right)+v_n\left(\mathbf{r}_1,t-\frac{r'}{c_0}\right)\cdot\frac{\partial}{\partial n}\left(\frac{1}{r'}\right)\right]ds\\
&=\frac{1}{2\pi}\int\int_S\left\{\left[\frac{1}{c_0r'}\cdot\frac{\partial}{\partial t}\,v_n\left(\mathbf{r}_1,t-\frac{r'}{c_0}\right)\right.\right.\\
&\quad\left.\left.+\frac{1}{r'^2}\cdot v_n\left(\mathbf{r}_1,t-\frac{r'}{c_0}\right)\right]\frac{\partial r'}{\partial n}\right\}ds,
\end{aligned} \tag{31}$$

where $r'=|\mathbf{r}'|=|\mathbf{r}_2-\mathbf{r}_1|$.

The surface element ds at the source surface in spherical coordinates is given as $ds=|\mathbf{r}_1|^2\sin\theta\,d\theta\,d\varphi$, where θ is the angle between $\mathbf{r}_1$ and z axis and φ is the angle between the projection of $\mathbf{r}_1$ on the xy plane and the x axis. As is shown in Fig. 2, $(\partial r'/\partial n)=\cos\gamma$, where γ is the angle between the $\mathbf{r}'$ and the z axis. Therefore, the normal particle velocity is given by:

$$\begin{aligned}
v_n(\mathbf{r}_2,t)=\frac{1}{2\pi}\int\int_S\left\{\left[\frac{1}{c_0r'}\cdot\frac{\partial}{\partial t}\,v_n\left(\mathbf{r}_1,t-\frac{r'}{c_0}\right)\right.\right.\\
\left.\left.+\frac{1}{r'^2}\cdot v_n\left(\mathbf{r}_1,t-\frac{r'}{c_0}\right)\right]\cdot\cos\gamma\right\}ds.
\end{aligned} \tag{32}$$

For this geometry, the Rayleigh integral for instantaneous pressure at point P of the intermediate plane can be rewritten as:

$$p(\mathbf{r}_2,t)=\frac{\rho}{2\pi}\int\int_S\left[\frac{1}{r'}\cdot\frac{\partial}{\partial t}\,v_n\left(\mathbf{r}_1,t-\frac{r'}{c_0}\right)\right]ds. \tag{33}$$

Equations (32) and (33) form the basic set of equations for simulating the effect of diffraction in our model. In discrete regime, the double integrals in Eqs. (32) and (33) were

solved numerically using a standard rectangular method.[34]

To obtain exact results, all calculations must be performed inside an extended volume which is a function of the geometrical characteristics of the source. This volume is defined as the envelope of a set of ellipsoids whose first foci are all placed on the source focal point and whose second foci are placed on different points of the source circular border. The eccentricity of these ellipsoids depends on the desired pulse length observed at the focal point (about 5 μs in our simulations).

The Rayleigh integral gives an exact solution to the diffraction problem for the case of a planar radiator in an infinite rigid baffle. Using this integral to simulate the effect of diffraction in our geometry therefore causes two kinds of errors: inherent and methodical. The inherent error relates to the geometry we used, i.e., a nonplanar source shape and a finite-baffle configuration. This source of error is not reducible. The methodical type of error is introduced by means of our fractional-step method. We studied the rate of this error for two different types of intermediate planes. In the first case, in our algorithm, we used the spherical-surface intermediate planes with the same center of curvature as the source, and in the second case, planar-surface intermediate planes were used. Comparison between these two different configurations revealed the superiority of the planar-surface intermediate planes. In fact, for this configuration, there exists a constant methodical error (about 3%) which is independent of the number of steps used, whereas for the spherical-surface plane configuration, this error is an increasing function of the number of steps (about 0.5% per step). The difference in the errors introduced by the two configurations of the intermediate planes is related to the fact that the solution of the Rayleigh integral over a curved surface introduces an error. When the planar-surface intermediate planes are used, this error is introduced only once, occurring only at the first step, i.e., from the source surface to the first intermediate plane. When the spherical-surface intermediate planes are used, however, a cumulative error is introduced at each step.

All simulations presented in the next sections were performed using the planar-surface intermediate planes.

V. FRACTIONAL-STEP METHOD WITH A SECOND-ORDER OPERATOR-SPLITTING ALGORITHM

The method of fractional steps with an operator-splitting algorithm has widely been used in numerical solutions to the problem of finite-amplitude sound beam propagation.[10–17] Besides, the technique was used in other physical problems, especially in optics.[35] A complete description of the technique can be found in Refs. 11 and 12. Using this method, we have developed a time-domain model for propagation of highly focused finite-amplitude ultrasonic beams by taking into account the effects of absorption, nonlinearity, and diffraction as independent phenomena. In this model, the acoustic beam propagates, plane-by-plane, from the surface of a highly focused spherical transducer up to its focus. The intermediate planes, all planar-surface type, are placed between the focused source and its focus. In each step, the abovementioned effects are applied sequentially: (1) by implementing the Rayleigh integral over the surface of the previous plane, the pressure and normal particle velocity are derived for each point of the current plane; (2) the effect of frequency-dependent absorption is applied to the pressure and normal particle velocity; (3) nonlinearly induced distortion is introduced to the resulted pressure and normal particle velocity to obtain the final values of these quantities for each point of the current plane; (4) code marches to the next step and the same procedure repeats.

The model was used to calculate the pressure field of an axisymmetric spherical highly focused piezocomposite shock-wave generator with an aperture diameter of 172 mm and with a 190-mm focal length (linear focusing gain $G \approx 30$, when driven by a sinusoidal pulse with a center frequency of 360 kHz). This source was developed in our laboratory for tissue destruction studies.[19,30] Because of the symmetry around the acoustical axis, in each observing plane, it is sufficient to calculate the acoustic field variables (instantaneous pressure and particle velocity) on a radial line, e.g., on x or y axes only.

In all simulations presented, the number of intermediate planes placed between the source front face and its focal point was set to be 23. This choice is a trade-off between the accuracy of calculations and the program run time. To have little changes of variable ν along each step Δz, as well as to avoid the problem of multivaluedness caused by nonlinear waveform steepening a nonuniform spacing was adopted: Axial step sizes were reduced by approaching the focus. Moreover, to satisfy inequality (27), especially in the region near the focus, after the first intermediate plane, each step was divided into 40 equally spaced substeps used only for nonlinearity calculation. Using this griding scheme, the minimum axial step sizes in the focal region were 2.02 mm for diffraction and absorption, and 50.5 μm for nonlinearity calculations. The number of surface elements, *ds*, for covering the surface of the source and each intermediate plane, was set to be 393 200, which is large enough to exactly calculate the Rayleigh integral: The minimum lateral step size in the focal region was about 2 μm.

The proper modeling of the shock fronts often requires a very dense temporal sampling. In our model, 5-μs pulses were sampled in 512-point vectors, i.e., with a sampling period less than 10 ns.

In the Appendix, we have proved a second-order accuracy operator-splitting algorithm used to solve numerically Eq. (8). In this algorithm there is a spatial shift between steps used for diffraction operation, $\hat{L}_D$, and those used for absorption, $\hat{L}_A$, and nonlinearity, $\hat{L}_N$, operations. Using this algorithm, it is possible to achieve a second order of accuracy with a running time not significantly higher than a first-order accuracy method. Figure 3(a) shows the basic geometry of nonuniform griding. Spatially shifted griding used for different operations in our second-order operator splitting method are shown schematically in Fig. 3(b).

At this time there is no analytical solution of the problem of beam propagation when multiple effects (diffraction, nonlinearity, absorption, etc.) are present. There is, therefore, no *a priori* reference to be used to assess the error from our

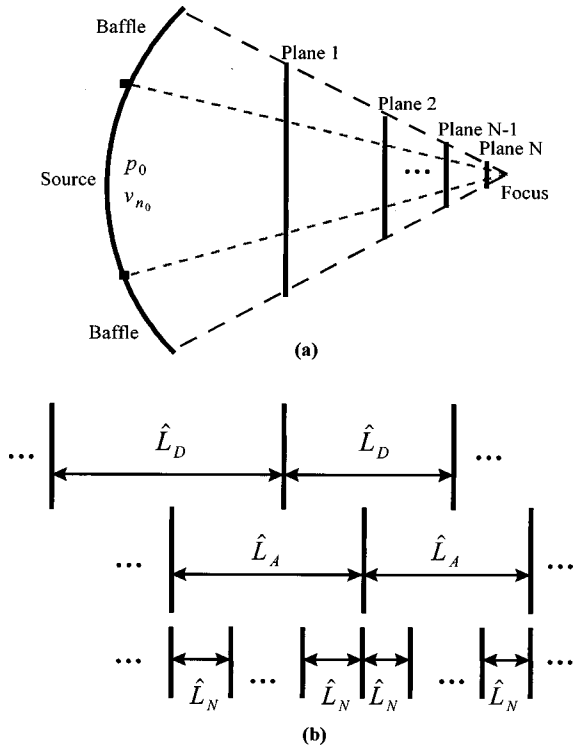

FIG. 3. (a) Axial griding scheme with nonuniform spacing; (b) spatially shifted griding for different operators in the second-order operator-splitting method.

numerical model. However, we investigated the stability of the code as a function of the number of steps. This study showed that the algorithm is convergent when the number of steps are increased (up to 79 intermediate planes). A similar study done by Lee and Hamilton to demonstrate the stability of their time-domain model for solving the KZK equation.[10]

An important characteristic of the operator-splitting method is that the final result is independent of the order of the effects when the steps Δz are small enough. To show this characteristic, we changed the order in which the effects (diffraction, absorption and nonlinearity) are applied in each plane. Specifically, we used two different orders:

Case 1: diffraction→absorption→nonlinearity

Case 2: absorption→nonlinearity→diffraction.

The discrepancy between the results of these two cases was reduced by increasing the number of planes. The maximum of the cross-correlation function was used as a criterion for comparing the waveforms obtained in each case. We studied the maximum of cross-correlation function applied to the pressure waveform as a function of number of the intermediate planes and for two different input pressures at source surface, i.e., $P_{\text{in}}=0.1$ MPa (linear regime) and $P_{\text{in}}=0.5$ MPa (nonlinear regime). This study showed that: even in nonlinear regime, by choosing a large enough number of planes, the maximum of the cross correlation would be close to 1 which shows that the algorithm is independent of the order of the effects. For example, for $P_{\text{in}}=0.5$ MPa and 17 intermediate planes, the maximum of cross correlation obtained was 0.991.[30]

TABLE I. Main acoustical parameters of water and 1,3-Butandiol.

	Water	1,3-Butandiol
Coefficient of attenuation (α_0)	0.0022 dB $\text{cm}^{-1}\,\text{MHz}^{-2}$	0.33 dB $\text{cm}^{-1}\,\text{MHz}^{-1}$
Frequency dependency of α	f^2	f^1
B/A	5.2	7.3
c_0	1500 m s^{-1}	1546 m s^{-1}
ρ	1000 kg m^{-3}	1000 kg m^{-3}

VI. NUMERICAL RESULTS AND COMPARISON WITH EXPERIMENTS

In this section, the results of implementing our numerical model and their comparisons with experimental results are presented. The initial version of the program was written in Matlab and then translated to C language and run on a Sun-UltraSparc workstation. For 23 intermediate planes and the griding scheme explained in the previous section, the program run time was about 3 h.

In Sec. VI A, the result of simulation for an ideal medium (linear and nondissipative) is presented. This simulation shows the validity of our model in linear regime. After verifying our algorithm in linear regime, we will present a series of simulation for real media by taking into account the effect of diffraction, absorption, and nonlinearity. The simulations, as well as experiments, were made for two different medium configurations. In the first configuration, an acoustic beam propagates from the source surface to its focus in degased and deionized water. In the second configuration, the propagation distance between the source front face and its focus is comprised of two parts. In the first part, the acoustic beam propagates from the source surface up to 5 cm from the focus in degased and deionized water, and in the second part, beam propagates the distance of 5 cm up to the focus in degased 1,3-Butandiol (ALDRICH, Steinheim, Germany) which is a tissue-mimicking liquid. These two medium configurations are called water and water-butandiol, respectively.[30] The relevant room temperature acoustical parameters of these media, as used in our simulations, are given in Table I.

A. Beam propagation in a linear and nondissipative medium

Here we present the simulation results for the propagation of a focused beam in an ideal medium, when only the effect of diffraction was accounted for. For this reason, the operator of nonlinearity, $\hat{L}_N$, was set to be zero, and only a small amount of absorption, $\hat{L}_A$, was introduced to provide stability of the numerical algorithm. In this simulation, input pressure at the surface of the transducer was considered as a Gaussian-modulated sinusoidal waveform with central frequency of 360 kHz and bandwidth of 120% [Fig. 4(a)]. The pressure calculations at the focus were made in two different cases. In the first case, using the linear wave theory, the pressure at the focus was calculated directly; i.e., without any intermediate plane; and in the second case, this pressure was calculated by means of our fractional-step method with 23 intermediate planes. These two pressure waveforms are presented in Fig. 4(b) and (c), respectively. The discrepancy

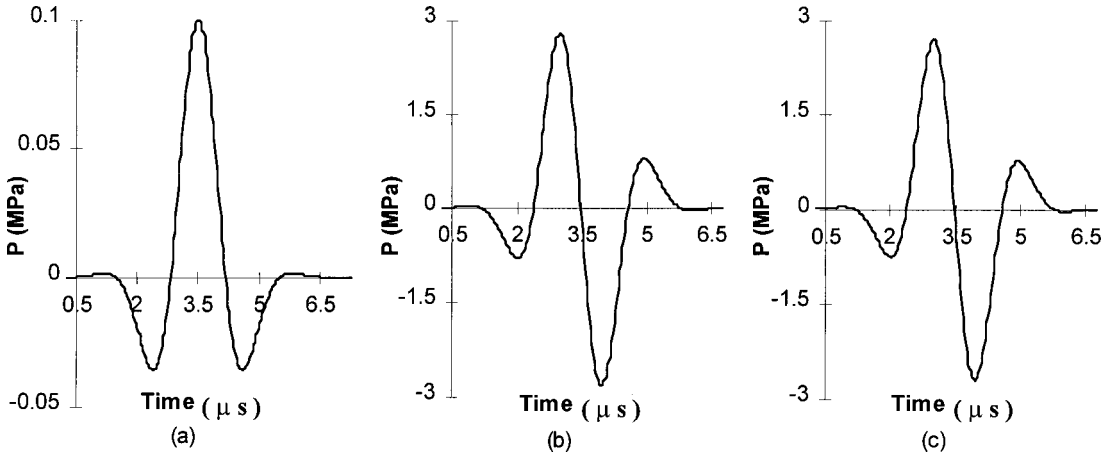

FIG. 4. Verifying the operator-splitting algorithm for the effect of diffraction. (a) Input pressure at the source surface; (b) calculated pressure waveform at the focus without any intermediate plane; and (c) with 23 intermediate planes.

between these two waveforms is about 3% for peak pressures which shows that it is possible to simulate the effect of diffraction quite accurately by means of our operator-splitting algorithm.

B. Pressure at the focal point in real media

Pressure-time waveforms at the focal point were calculated for different input pressure amplitudes at the source surface. For all of the simulations presented here and those that follow, the input pressure is the same as that measured at the surface of the generator using a PVDF bilaminar shielded membrane hydrophone.[19,30] Figures 5 and 6 show the calculated and measured pressure-time waveforms at the focus for the second configuration of the medium, i.e., water-butandiol, and for two different input pressure amplitudes (P_{in}=0.476 and 0.85 MPa). The presence of the nonlinearly induced shock fronts are notable in Fig. 6. For pressure measurements at the focus, a homemade PVDF shock-wave hydrophone was used.[36]

Comparison between the calculated and measured waveforms shows a very good agreement in the shape of waveforms. However, there exists some discrepancy between the pressure amplitudes. The maximum of this discrepancy was around 20% for positive pressure amplitudes. In the conclusion and discussion section, the sources of this discrepancy will be discussed.

Figure 7 shows the variations of the positive peak pressure at the focus as a function of input pressure amplitude at

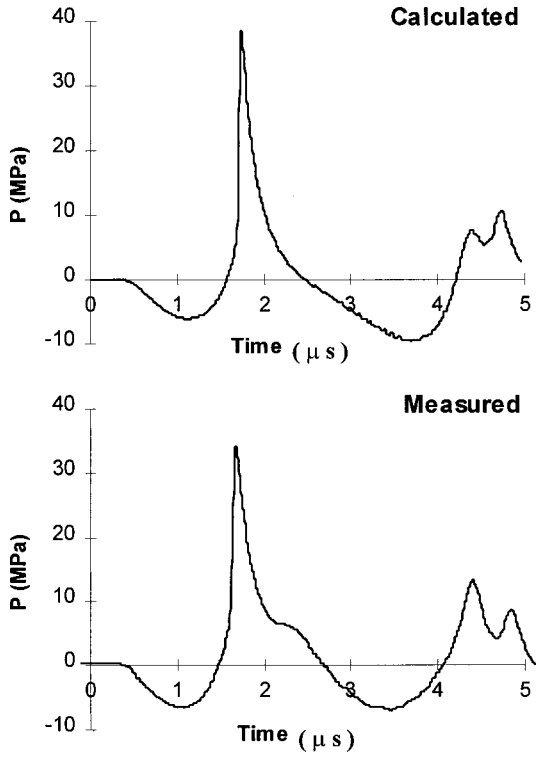

FIG. 5. Calculated and measured pressure-time waveforms at the focal point for P_{in}=0.476 MPa.

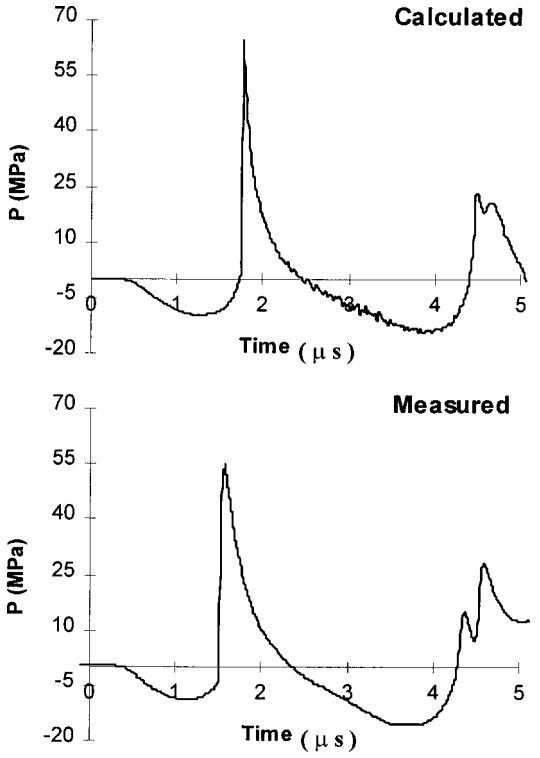

FIG. 6. Calculated and measured pressure-time waveforms at the focal point for P_{in}=0.85 MPa.

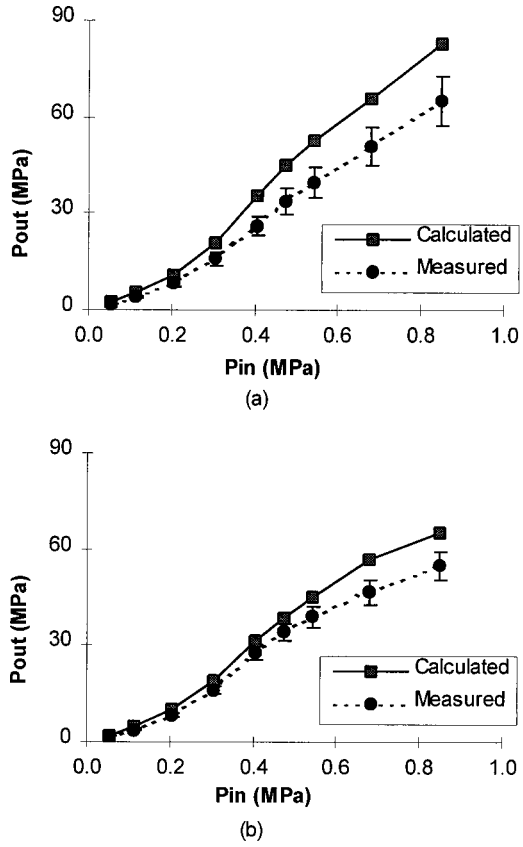

FIG. 7. Output pressure amplitude at the focus as a function of input pressure amplitude at the source surface for two medium configurations: (a) water; and (b) water-butandiol.

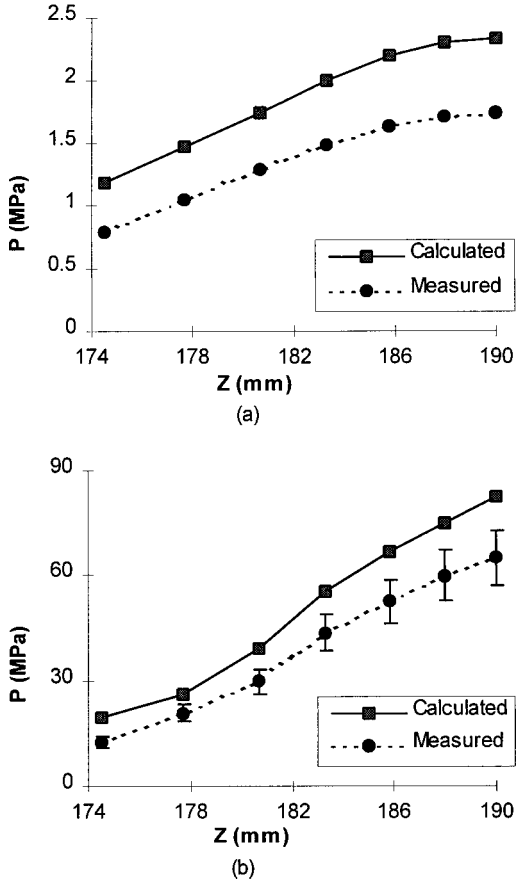

FIG. 8. On-axis pressure distributions in water. (a) $P_{in}=0.056$ MPa (linear regime); and (b) $P_{in}=0.85$ MPa (nonlinear regime).

the source surface for two medium configurations. For each medium, the results of theory and experiments have been shown. Both the theoretical and experimental results show three distinct regions of variations as: (1) acoustic pressure at the focus varies as a linear function of input pressure for very low input excitation levels ($P_{in}<0.1$ MPa); (2) for moderate levels of input pressures, there is an increase in slope of this variation (0.1 MPa$<P_{in}<0.4$ MPa); (3) and finally for high levels of input excitation, this slope decreases ($P_{in}>0.4$ MPa). The discrepancy between the theory and experiment increases by increasing the input pressure amplitude. This discrepancy may be explained by the pressure-averaging effect over the surface of the hydrophone active element that is larger than the real focus size. Increasing the input pressure amplitude leads to amplification of the nonlinearity effect with creation of the higher harmonics, and consequently to contraction of the focus size. The pressure-averaging effect over the surface of the hydrophone active element, therefore, becomes more important for higher input pressures.

C. On- and off-axis pressure distributions

Using our model, it is possible to simulate the plane-by-plane beam propagation in a medium. This simulation in linear regime shows that the waveform is mainly affected by diffraction which leads to a linear amplification of pressure during its propagation. In nonlinear regime, however, the situation is not so simple. Here, the nonlinearly induced wave distortion which leads to the creation of very steep shock fronts with higher harmonics in the signal spectrum, causes nonlinear amplification of the pressure. Also, the effect of frequency-dependent absorption becomes more important in this case.

Figures 8 and 9 show the theoretical and experimental on- and off-axis pressure distributions around the focus in water. These distributions are presented for both the linear ($P_{in}=0.056$ MPa) and nonlinear ($P_{in}=0.85$ MPa) regimes. Again, a good agreement between the theory and experiment is obvious. These distributions reveal the contraction of the focus dimensions in nonlinear regime.

VII. CONCLUSION AND DISCUSSION

In this work, we have presented a time-domain model for calculating the acoustic field of a finite-amplitude, highly focused source in pulsed regime. In this model, the main effects responsible in finite-amplitude beam propagation in a dissipative medium were taken into account. These effects, considered as independent phenomena, are: absorption, nonlinearity, and diffraction. Using general wave theory, we derived separate evolution-type differential equations for each of these effects and by combining these separate equations, the final evolution equation was derived in the form of Eq. (8). This equation was solved numerically, using the operator-splitting method.

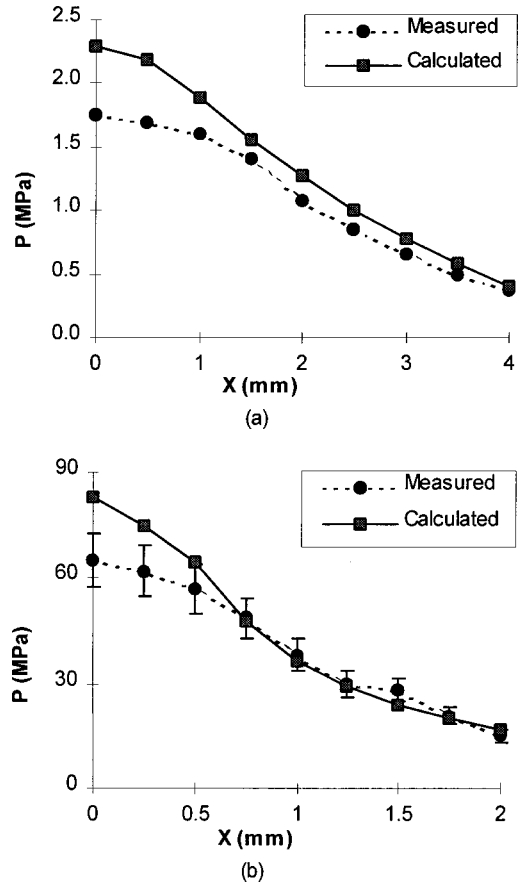

FIG. 9. Off-axis pressure distributions in water. (a) $P_{in}=0.056$ MPa (linear regime); and (b) $P_{in}=0.85$ MPa (nonlinear regime).

To solve the frequency-dependent attenuation equation, a minimum-phase digital filter model was developed. To be a causal filter, the log-magnitude and phase characteristics form a Hilbert transform pair. Using this filter model, the frequency-dependent attenuation and dispersion were exactly simulated without any waveform distortion even for a shock-wave pulse.

To simulate the effect of nonlinearity, we used the evolution equation for a plane wave propagating in an ideal quadratically nonlinear medium. Based on the analytical solution of this equation, the nonlinearly induced wave distortion was simulated via a simple time-base transformation.

To obtain an exact formulation of diffraction, we used the Rayleigh integral. The results of calculation in an ideal, linear, and nondissipative medium show the validity of our algorithm to simulate exactly the effect of diffraction. Full diffraction formulation enables our model to be used for simulating the finite-amplitude acoustic field of highly focused sources.

In a real medium, i.e., by taking into account the effects of diffraction, absorption, and nonlinearity, very good agreement was obtained in the shape of theoretical and experimental pressure waveforms. The discrepancy in the amplitudes may be explained by existing sources of error in our measurements from one hand and in the theoretical model on the other hand. The main sources of uncertainty in our measurements are: pressure-averaging effect over the surface of the hydrophone active element, error in the measured value of the shockwave hydrophone sensitivity,[36] and error in the measurement of the generator electro-acoustical conversion factor at its source surface.[30,37] Among these, we believe that the first one, i.e., the effect of pressure averaging over the surface of hydrophone active element, has had the most important influence on our measurements, especially in nonlinear regime when the focus dimensions become comparable with, or even smaller than, the hydrophone active element size ($\Phi=1$ mm in our measurements). To obtain an idea of the influence of this averaging effect on our results, we made a simple simulation in nonlinear regime and in water. In this simulation, based on calculated off-axis pressure distribution presented in Fig. 9, we derived the pressure amplitudes at 20 equally spaced points in the focal plane and on the *x*-axis, from the focus to a distance of 0.5 mm from the focus. We consider a circular-shape hydrophone active element with a radius of 0.5 mm. If the center of the hydrophone active element is placed at the focus, by dividing the active element area into 20 concentric and equal-width annuli, we can calculate the averaged value of the pressure by averaging the pressures at different annuli with the scaling factors proportional to the surface of each annulus. Using this method, the averaged pressure over the hydrophone active element in nonlinear regime ($P_{in}=0.85$ MPa) and in water was found to be about 11% smaller than the calculated pressure. As a result, we can conclude that a major part of the 20% discrepancy observed between the theory and experiments may be related to the averaging effect over the hydrophone active element.

The time-domain numerical model presented in this work can be used as a fairly simple theoretical tool for studying the intensive highly focused acoustic beam propagation in different medium configurations with a symmetrical source geometry. The technique has some advantages over other time-domain methods in the literature in that it allows (1) for arbitrary absorption and dispersion, and (2) does not make use of the parabolic approximation for diffraction. The latter point is particularly important because the trend in biomedical research is toward highly focused, intensive sources, and many current models cannot account for high focusing gains.

In the model presented, we have not considered the effects of reflection and refraction. These effects may have an important influence on wave propagation especially in multilayered media which cause an overestimation in the results of the simulation. The media used in this study (water and butandiol) have practically the same values of acoustic impedances and sound velocities: This source of error is therefore negligible in the results presented here.

Adding the effects of reflection and refraction, this model can be used to simulate the wave propagation in multi-layered media, such as a simplified model for the human body. Another field of application is to study electronic focusing along the acoustical axis of a high-amplitude two-dimensional focused source. Our method can easily be extended to asymmetrical sources, that makes it possible to simulate the focused finite-amplitude wave propagation in a medium with presence of arbitrary obstacles in the path of

propagation, as well as simulation of on- and off-axis electronic beam steering.

ACKNOWLEDGMENTS

The authors gratefully acknowledge the suggestions of Dr. Richard S. C. Cobbold, and wish to thank Dr. Valery P. Kandidov for discussions on the method of fractional steps. We also appreciate assistance of Brian Lim in reviewing the manuscript.

APPENDIX

Here, we describe and prove a second-order accuracy operator-splitting algorithm. For this reason, we calculate the solution of Eq. (8) at distance $z+\Delta z$ on the basis of the waveform ν at distance z within three steps:

Step 1. We consider the evolution equation (6) for diffraction:

$$\frac{\partial \nu_1}{\partial z}=\hat{L}_D \nu_1, \tag{A1}$$

with initial condition $\nu_1(z)=\nu_0$. As the first step, we calculate the waveform ν_1 at the distance $z+\Delta z/2$. Using a Taylor series expansion, it is possible to write:

$$\nu_1\left(z+\frac{\Delta z}{2}\right)=\nu_1(z)+\frac{\Delta z}{2}\cdot\frac{\partial \nu_1(z)}{\partial z}+\frac{\Delta z^2}{8}\cdot\frac{\partial^2 \nu_1(z)}{\partial z^2}+O(\Delta z^3). \tag{A2}$$

Note that within the Rayleigh integral approximation, the differential operator $\partial/\partial z$ commutes with the diffraction operator $\hat{L}_D$:

$$\frac{\partial}{\partial z}\hat{L}_D \nu_1(z)=\hat{L}_D\frac{\partial \nu_1(z)}{\partial z}. \tag{A3}$$

Indeed, the Rayleigh integral (32) represents an exact solution of the wave equation

$$\nabla^2 \nu-\frac{1}{c_0^2}\cdot\frac{\partial^2 \nu}{\partial t^2}=0$$

in case of the plane surface of integration, when the normal to the surface does not depend on coordinates. In our model, all intermediate observing planes are parallel with the *xy* plane, so $\partial/\partial z=\partial/\partial n$ over the surface of these planes (Fig. 2). In the case of $\vec{n}=\text{const}$, we obtain from the wave equation that the derivative $\partial v/\partial z$ is also a solution of the wave equation, so the integral (32) is valid for it. This proves that the diffraction operator $\hat{L}_D$ commutes with the differential operator $\partial/\partial z$. Using the result (A3), we obtain from Eqs. (A1) and (A2):

$$\nu_1\left(z+\frac{\Delta z}{2}\right)=\nu_0+\frac{\Delta z}{2}\hat{L}_D\nu_0+\frac{\Delta z^2}{8}\hat{L}_D^2\nu_0+O(\Delta z^3). \tag{A4}$$

Step 2. Consider the following evolution equation for the effects of absorption and nonlinearity:

$$\frac{\partial \nu_2}{\partial z}=\hat{L}_A\nu_2+\hat{L}_N\nu_2, \tag{A5}$$

with initial condition $\nu_2(z)=\nu_1(z+\Delta z/2)$. As the second step, we calculate the waveform ν_2 at distance $z+\Delta z$. The Taylor series expansion gives:

$$\nu_2(z+\Delta z)=\nu_2(z)+\Delta z\frac{\partial v_2(z)}{\partial z}+\frac{\Delta z^2}{2}\cdot\frac{\partial^2 \nu_2(z)}{\partial z^2}+O(\Delta z^3). \tag{A6}$$

Note, that according to Eq. (3) the differential operator $\partial/\partial z$ commutes with the operator $\hat{L}_A$, i.e.:

$$\frac{\partial}{\partial z}\hat{L}_A\nu_2(z)=\hat{L}_A\frac{\partial \nu_2(z)}{\partial z}. \tag{A7}$$

However, this is not the case for operators $\partial/\partial z$ and $\hat{L}_N$ in Eq. (4). Let us introduce a linear operator $\hat{\Lambda}_N=(\beta/2c_0^2)\times(\partial/\partial\tau)$, such that:

$$\hat{L}_N\nu_2=\hat{\Lambda}_N\nu_2^2. \tag{A8}$$

The operator $\hat{\Lambda}_N$ commutes with $\partial/\partial z$, therefore:

$$\frac{\partial}{\partial z}\hat{L}_N\nu_2(z)=2\hat{\Lambda}_N\left[\nu_2\frac{\partial \nu_2(z)}{\partial z}\right]. \tag{A9}$$

Equations (A4) to (A9) give the following expansion for the waveform ν_2 at distance $z+\Delta z$:

$$\begin{aligned}\nu_2(z+\Delta z)&=\nu_0+\Delta z\cdot\left[\tfrac{1}{2}\hat{L}_D\nu_0+\hat{L}_A\nu_0+\hat{\Lambda}_N\nu_0^2\right]\\&+\frac{\Delta z^2}{2}\cdot\left[\frac{1}{4}\hat{L}_D^2\nu_0+\hat{L}_A\hat{L}_D\nu_0+2\hat{\Lambda}_N(\nu_0\hat{L}_D\nu_0)+\hat{L}_A^2\nu_0\right]\\&+\frac{\Delta z^2}{2}\cdot\left[\hat{L}_A\hat{\Lambda}_N\nu_0^2+2\hat{\Lambda}_N(\nu_0\hat{L}_A\nu_0)+2\hat{\Lambda}_N(\nu_0\hat{\Lambda}_N\nu_0^2)\right]\\&+O(\Delta z^3).\end{aligned} \tag{A10}$$

Step 3. Consider Eq. (A1) again:

$$\frac{\partial \nu_3}{\partial z}=\hat{L}_D\nu_3, \tag{A11}$$

with initial condition $\nu_3(z+\Delta z/2)=\nu_2(z+\Delta z)$. As the third step, we calculate the waveform ν_3 at distance $z+\Delta z$. Using the Taylor series expansion, it is possible to write:

$$\nu_3(z+\Delta z)=\nu_3(z+\Delta z/2)+\frac{\Delta z}{2}\cdot\frac{\partial \nu_3(z+\Delta z/2)}{\partial z}+\frac{\Delta z^2}{8}\cdot\frac{\partial^2 \nu_3(z+\Delta z/2)}{\partial z^2}+O(\Delta z^3). \tag{A12}$$

Taking into account Eq. (A3), we obtain from Eqs. (A10) to (A12):

$$v_3(z+\Delta z)=v_0+\Delta z\cdot[\hat{L}_D v_0+\hat{L}_A v_0+\hat{\Lambda}_N v_0^2]$$
$$+\frac{\Delta z^2}{2}\cdot[\hat{L}_D^2 v_0+\hat{L}_D\hat{L}_A v_0+\hat{L}_A\hat{L}_D v_0$$
$$+\hat{L}_D\hat{\Lambda}_N v_0^2+\hat{L}_A^2 v_0+\hat{L}_A\hat{\Lambda}_N v_0^2]$$
$$+\frac{\Delta z^2}{2}\cdot[2\hat{\Lambda}_N(v_0\hat{L}_D v_0)+2\hat{\Lambda}_N(v_0\hat{L}_A v_0)$$
$$+2\hat{\Lambda}_N(v_0\hat{\Lambda}_N v_0^2)+O(\Delta z^3). \quad \text{(A13)}$$

Let $v(z)=v_0$, the following expression for the waveform at distance $z+\Delta z$ results from the evolution equation (8):

$$v(z+\Delta z)=v(z)+\Delta z\,\frac{\partial v(z)}{\partial z}+\frac{\Delta z^2}{2}\cdot\frac{\partial^2 v(z)}{\partial z^2}+O(\Delta z^3)$$
$$=v_0+\Delta z\cdot[\hat{L}_D v_0+\hat{L}_A v_0+\hat{\Lambda}_N v_0^2]$$
$$+\frac{\Delta z^2}{2}\cdot[\hat{L}_D^2 v_0+\hat{L}_D\hat{L}_A v_0+\hat{L}_A\hat{L}_D v_0+\hat{L}_D\hat{\Lambda}_N v_0^2$$
$$+\hat{L}_A^2 v_0+\hat{L}_A\hat{\Lambda}_N v_0^2]$$
$$+\frac{\Delta z^2}{2}\cdot[2\hat{\Lambda}_N(v_0\hat{L}_D v_0)+2\hat{\Lambda}_N(v_0\hat{L}_A v_0)$$
$$+2\hat{\Lambda}_N(v_0\hat{\Lambda}_N v_0^2)]+O(\Delta z^3). \quad \text{(A14)}$$

Comparing Eqs. (A13) and (A14), we conclude:

$$v(z+\Delta z)=v_3(z+\Delta z)+O(\Delta z^3), \quad \text{(A15)}$$

which proves the operator-splitting algorithm with the second-order of accuracy.

[1] L. Germain and J. D. N. Cheeke, ''Generation and detection of high-order harmonics in liquids using a scanning acoustic microscope,'' J. Acoust. Soc. Am. **83**, 942–949 (1988).

[2] J. Y. Chapelon and D. Cathignol, ''High energy ultrasound therapy: Part I—High intensity focused ultrasound (HIFU),'' in *Advances in Nonlinear-Acoustics*, edited by H. Hobaek, 13th International Symposium on Nonlinear Acoustics, Bergen, 28 June–2 July 1993 (World Scientific, Singapore, 1993), pp. 21–29.

[3] D. Cathignol and J. Y. Chapelon, ''High energy ultrasound therapy: Part II—Shock waves and cavitation,'' in *Advances in Nonlinear Acoustics*, edited by H. Hobaek, 13th International Symposium on Nonlinear Acoustics, Bergen, 28 June–2 July 1993 (World Scientific, Singapore, 1993), pp. 30–35.

[4] E. A. Zabolotskaya and R. V. Khokhlov, ''Quasi-plane waves in the nonlinear acoustics of confined beams,'' Sov. Phys. Acoust. **15**, 35–40 (1969).

[5] V. P. Kuznetsov, ''Equations of nonlinear acoustics,'' Sov. Phys. Acoust. **16**, 467–470 (1971).

[6] J. Naze Tjøtta, S. Tjøtta, and E. H. Vefring, ''Propagation and interaction of two collimated finite amplitude sound beams,'' J. Acoust. Soc. Am. **88**, 2859–2870 (1990).

[7] J. Naze Tjøtta, S. Tjøtta, and E. H. Vefring, ''Effects of focusing on the nonlinear interaction between two collinear finite amplitude sound beams,'' J. Acoust. Soc. Am. **89**, 1017–1027 (1991).

[8] S. I. Aanonsen, ''Numerical computation of the nearfield of a finite amplitude sound beam,'' Tech. Rep. No. 73, Department of Mathematics, University of Bergen, Bergen, Norway (1983).

[9] S. I. Aanonsen, T. Barkve, J. Naze Tjøtta, and S. Tjøtta, ''Distortion and harmonic generation in the nearfield of a finite amplitude sound beam,'' J. Acoust. Soc. Am. **75**, 749–768 (1984).

[10] Y. S. Lee and M. F. Hamilton, ''Time-domain modeling of pulsed finite-amplitude sound beams,'' J. Acoust. Soc. Am. **97**, 906–917 (1995).

[11] W. F. Ames, *Numerical Methods for Partial Differential Equations* (Academic, San Diego, 1992), 3rd ed.

[12] W. H. Press, S. A. Teukolsky, W. T. Vetterling, and B. P. Flannery, *Numerical Recipes in FORTRAN* (Cambridge U.P., New York, 1992), 2nd ed., pp. 847–848.

[13] R. O. Cleveland, M. F. Hamilton, and D. T. Blackstock, ''Time-domain modeling of finite-amplitude sound in relaxing fluids,'' J. Acoust. Soc. Am. **99**, 3312–3318 (1996).

[14] M. A. Averkiou and M. F. Hamilton, ''Nonlinear distortion of short pulses radiated by plane and focused circular pistons,'' J. Acoust. Soc. Am. **102**, 2539–2548 (1997).

[15] R. O. Cleveland, J. P. Chambers, H. E. Bass, R. Raspet, D. T. Blackstock, and M. F. Hamilton, ''Comparison of computer codes for the propagation of sonic boom waveforms through isothermal atmospheres,'' J. Acoust. Soc. Am. **100**, 3017–3027 (1996).

[16] P. T. Christopher and K. J. Parker, ''New approaches to nonlinear diffractive field propagation,'' J. Acoust. Soc. Am. **90**, 488–499 (1991).

[17] T. Christopher, ''Modeling the Dornier HM3 lithotripter,'' J. Acoust. Soc. Am. **96**, 3088–3095 (1994).

[18] D. Cathignol, O. A. Sapozhnikov, and J. Tavakkoli, ''One-dimensional theoretical model of high-intensity pulse focusing,'' in *Nonlinear Acoustics in Perspective*, edited by R. J. Wei, 14th International Symposium on Nonlinear Acoustics (Nanjing U.P., Nanjing, 1996), pp. 177–182.

[19] J. Tavakkoli, A. Birer, A. Arefiev, F. Prat, J. Y. Chapelon, and D. Cathignol, ''A piezocomposite shock wave generator with electronic focusing capability: Application for producing cavitation-induced lesions in rabbit liver,'' Ultrasound Med. Biol. **23**, 107–115 (1997).

[20] O. V. Rudenko and S. I. Soluyan, *Theoretical Foundations of Nonlinear Acoustics* (Plenum, New York, 1977).

[21] V. G. Andreev, V. A. Khokhlova, O. V. Rudenko, and O. A. Sapozhnikov, ''Suppression of nonlinear damping of a sound wave in a medium which contains a resonant absorber with a finite line width,'' Mosc. Univ. Phys. Bull. (USA), No. 3, 67–71 (1985).

[22] R. J. Hill, ''Wider-angle parabolic wave equation,'' J. Acoust. Soc. Am. **79**, 1406–1409 (1986).

[23] J. W. Strutt (Lord Rayleigh), *Theory of Sound* (Dover, New York, 1945), Vol. 2.

[24] H. T. O'Neil, ''Theory of focusing radiators,'' J. Acoust. Soc. Am. **21**, 516–526 (1949).

[25] A. Penttinen and P. M. Luukkala, ''The impulse response and pressure near field of a curved ultrasonic radiator,'' J. Phys. D **9**, 1547–1557 (1976).

[26] A. V. Oppenheim and R. W. Schafer, *Digital Signal Processing* (Prentice-Hall, London, 1975).

[27] M. O'Donnell, E. T. Jaynes, and J. G. Miller, ''Kramers-Kronig relationship between ultrasonic attenuation and phase velocity,'' J. Acoust. Soc. Am. **69**, 696–701 (1981).

[28] R. Kuc, ''Digital filter models for media having linear with frequency loss characteristics,'' J. Acoust. Soc. Am. **69**, 35–40 (1981).

[29] R. Kuc, ''Generating a minimum-phase digital filter model for the acoustic attenuation of soft tissue,'' 1983 Ultrasonics Symposium: Proceedings, 794–796 (1983).

[30] J. Tavakkoli, ''Study of intensive focused ultrasonic pulse propagation in biological media: application to shock wave-induced tissue destruction *in vitro* and *in vivo*,'' Ph.D. dissertation (English version), No. 65–97, University of Claude Bernard—Lyon 1 (1997).

[31] M. F. Hamilton and D. T. Blackstock, *Nonlinear Acoustics* (Academic, San Diego, 1998).

[32] R. T. Beyer, *Nonlinear Acoustics* (U.S. Naval Sea Systems Command, Washington, 1974).

[33] J. Lelong, ''Contribution à l'étude d'un dispositif piézo-électrique de puissance en vue de la creation d'ondes de choc,'' Ph. D. thesis, University of Pierre et Marie Curie—Paris VI, 1990.

[34] E. Kreyszig, *Advanced Engineering Mathematics* (Wiley, New York, 1979), Chap. 19.

[35] J. Martin, ''Simulation of wave propagation in random media: theory and application,'' in *Wave Propagation in Random Media (Scintillation)* (SPIE, Philadelphia, 1992), SPIE PM-09, pp. 463–486.

[36] J. Tavakkoli, A. Birer, and D. Cathignol, ''Development of a PVDF low-cost shock-wave hydrophone,'' Shock Waves **5**, 369–374 (1996).

[37] D. Cathignol, A. Birer, S. Nachef, and J. Y. Chapelon, ''Electronic beam steering of shock waves,'' Ultrasound Med. Biol. **3**, 365–377 (1995).